RM L52J27a

NACA

RESEARCH MEMORANDUM

A SIMPLIFIED MATHEMATICAL MODEL FOR CALCULATING AERODYNAMIC LOADING AND DOWNWASH FOR MIDWING WING-FUSELAGE COMBINATIONS WITH WINGS OF ARBITRARY PLAN FORM

By Martin Zlotnick and Samuel W. Robinson, Jr.

Langley Aeronautical Laboratory
Langley Field, Va.

NATIONAL ADVISORY COMMITTEE
FOR AERONAUTICS

WASHINGTON

January 16, 1953

NATIONAL ADVISORY COMMITTEE FOR AERONAUTICS

RESEARCH MEMORANDUM

A SIMPLIFIED MATHEMATICAL MODEL FOR CALCULATING AERODYNAMIC LOADING AND DOWNWASH FOR MIDWING WING-FUSELAGE COMBINATIONS WITH WINGS OF ARBITRARY PLAN FORM

By Martin Zlotnick and Samuel W. Robinson, Jr.

SUMMARY

It is shown that, for the purpose of calculating aerodynamic loads on the fuselage, the midwing wing-fuselage combination in subsonic flow can be represented by a simple system of horseshoe vortices located on the wing with images located inside the fuselage. Using this simplified mathematical model, a method for calculating the lift and longitudinal center of pressure on the fuselage in the presence of the wing is presented.

In addition it is shown how the simplified mathematical model can be used for calculating the downwash behind the wing and for calculating the spanwise lift distribution on the wing in the presence of the fuselage.

INTRODUCTION

Mutual interference between wing and fuselage has a significant effect on the pitching moment of the wing-fuselage combination since the longitudinal distribution of the aerodynamic loading on the fuselage is altered by the presence of the wing. For configurations with unswept wings Multhopp (ref. 1) has developed a theoretical method for calculating the pitching moment on wing-fuselage combinations which gives good agreement with experimental results. However, for calculating the pitching moment on swept-wing configurations, only semiempirical methods such as that of reference 2 are available.

The aerodynamic loading on the fuselage in subsonic flow is considered in references 1 and 2 to be made up of two parts. The first part, which is due to the fuselage angle of attack resulting from both the fuselage geometric angle of attack and the upwash angle induced by the wing,

has been calculated in reference 1 for straight-wing configurations and modified in reference 2 for the swept-wing case. The second part, which is often referred to as the wing lift "carried over" by the fuselage (which will be referred to in this paper as the induced lift), has been calculated analytically for the straight-wing case by Multhopp. However, for swept wings Multhopp's calculation cannot be applied and no other theoretical method has been available. In reference 2 this component of loading is estimated by an empirical method.

In order to calculate the induced lift on the fuselage in combination with a wing of arbitrary plan form, a method is suggested in the present paper which is based on Lennertz's (ref. 3) theoretical work. Lennertz's results, which are concerned only with an unswept lifting line passing through the axis of an infinitely long cylindrical fuselage, are, in effect, generalized so that in subsonic flow the magnitude and center of pressure of the induced lift on the fuselage when combined with a swept lifting line, or even a lifting surface, can be calculated. A numerical example is given in the appendix to illustrate the method. The effect of finite fuselage length is estimated qualitatively from results of an approximate calculation of the variation with slenderness ratio of the induced lift on an ellipsoid of revolution combined with an infinite vortex. The approximate calculation is shown to give results which agree with results of Vandrey (ref. 4).

In calculating the induced lift on the infinitely long fuselage, the wing-fuselage combination is replaced by a simple system of horseshoe vortices (or doublets) on the wing, with images inside the fuselage. This representation may also be used, with some modifications, in calculating the lift on the wing in the presence of the fuselage and also the corresponding downwash. However, for calculating the downwash and the lift on the wing, the simplified representation of the wing-fuselage combination, although it is considered to be adequate, is no longer rigorous, and the general applicability will depend on experimental verification.

SYMBOLS

A	aspect ratio (wing alone)
a	maximum radius of body of revolution
b	wing span
c	wing chord
$\bar{c}$	mean chord, S/b

c_l local lift coefficient

d major axis of ellipsoid of revolution

L_f total lift on the fuselage

p pressure

q dynamic pressure

S wing area (wing alone)

s semispan of bound leg of horseshoe vortex

U_∞ free-stream velocity

U_{max} maximum longitudinal velocity on surface of body

x_{cp} longitudinal center of pressure

Γ_b vortex strength

γ spanwise loading coefficient on wing, $cc_l/\bar{c}$

ρ mass density

Subscript:

n particular pair of horseshoe vortices

A prime denotes that the quantity is dimensionless with respect to a; an asterisk denotes that the quantity is dimensionless with respect to b/2; and a bar over a symbol denotes that the quantity is dimensionless with respect to s.

BASIC CONSIDERATIONS

Midwing Configurations With Axisymmetrical Fuselages

In the major part of the analysis the fuselage is assumed to be an infinite cylinder. To obtain a qualitative estimate of the effect of the finite fuselage length, the variation with slenderness ratio of the lift on an ellipsoid of revolution with a wing of infinite span will be calculated approximately in one of the following sections. An approximate method for making the small correction for this effect will be indicated.

Review of results obtained by Lennertz.- Lennertz (ref. 3) has calculated the lateral and longitudinal lift distribution on the fuselage of an idealized wing-fuselage configuration, in which the fuselage was represented by an infinite circular cylinder and the wing by a vortex having constant spanwise circulation. The vortices trailing from the wing tips have images inside the cylinder, and the bound vortex is extended inside the cylinder to join the trailing image vortices as shown in figure 1. With this configuration, the boundary condition on the cylinder of zero velocity normal to the surface is satisfied only at infinity and in the plane normal to the cylinder axis which passes through the vortex so that it is necessary to superimpose an additional potential, which Lennertz calculated. For this case the lateral lift distribution was obtained by considering the momentum change in a vertical plane infinitely far behind the wing, and the longitudinal lift distribution was obtained by the use of Bernoulli's equation.

Induced lift on an infinite cylinder with a finite wing having constant spanwise circulation distribution.- It will be shown that the fuselage lift L_f and its lateral distribution dL_f/dy are not affected by the additional potential so that only the components of L_f and dL_f/dy due to the vortex potential need be calculated.

Neglecting all other singularities, the lift on a longitudinal section of the cylinder dy (see fig. 1) due to the vortex potential is calculated as follows:

The pressure p of any point on the surface of the cylinder can be written

$$p = p_o + \frac{1}{2}\rho\left[\left(U_\infty + \Delta u\right)^2 + \Delta v^2 + \Delta w^2\right]$$

where Δu, Δv, and Δw are, respectively, the longitudinal, lateral, and vertical components of velocity induced by the vortices. The section lift dL_f/dy is then written

$$\frac{dL_f}{dy} = \int_{-\infty}^{\infty} \left(p_u - p_l\right) dx$$

where p_u and p_l are the pressures on the upper and lower surfaces, respectively.

Then

$$\frac{dL_f}{dy} = 2\rho U_\infty \int_{-\infty}^{\infty} \Delta u \, dx \tag{1}$$

Only the velocities induced by the bound vortex contribute to the lift.

It may be noted that, since the distribution of the longitudinal velocities induced by the bound vortex is symmetrical about its axis at every section dy, the longitudinal center of pressure of the lift due to the vortex potential is on the axis of the bound vortex.

A closed expression for the integral in equation (1) may be readily derived as follows: Consider the rectangular path indicated by the dashed line in the upper right sketch in figure 1 and the cross section downstream at infinity shown in the lower right sketch of the same figure. The line integral of the tangential velocity component, taken around the complete rectangle, $\oint \Delta u \, ds$ must be Γ_b where the path links one of the horseshoe vortices $\left(\left|\frac{a^2}{b/2}\right| < |y| < |a|\right)$, and must be zero where it does not link one of the horseshoe vortices $\left(0 < |y| < \left|\frac{a^2}{b/2}\right|\right)$. Then the desired integral in equation (1), which is the longitudinal portion of the complete line integral $\oint \Delta u \, ds$, must equal $\oint \Delta u \, ds$ minus the line integral along the short vertical line at infinity $\int_u^l \Delta w(\infty,y,z)dz$, where u refers to the upper surface and l refers to the lower surface. The integral $\int_{-\infty}^{\infty} \Delta u \, dx$ is

$$\int_{-\infty}^{\infty} \Delta u \, dx = \oint \Delta u \, ds - \int_u^l \Delta w(\infty,y,z)dz \tag{2}$$

Since

$$\Delta w = -\frac{\partial \phi}{\partial z}$$

then

$$\int_u^l \Delta w \, dz = \phi_u - \phi_l$$

where ϕ_u and ϕ_l are the potentials on the upper and lower surfaces, respectively, in the plane $x = \infty$. When $\left|\frac{a^2}{b/2}\right| < |y| < |a|$,

$$\phi_u = -\phi_l = \frac{\Gamma_b}{2\pi}\left(\tan^{-1}\frac{\sqrt{a^2 - y^2}}{y - \frac{b}{2}} - \tan^{-1}\frac{\sqrt{a^2 - y^2}}{y + \frac{b}{2}} - \tan^{-1}\frac{\sqrt{a^2 - y^2}}{y - \frac{a^2}{b/2}} + \tan^{-1}\frac{\sqrt{a^2 - y^2}}{y + \frac{a^2}{b/2}}\right) = \frac{1}{\pi}\Gamma_b\left[\tan^{-1}\frac{2\frac{b}{2}\sqrt{a^2 - y^2}}{\left(\frac{b}{2}\right)^2 - a^2}\right]$$

and

$$\oint \Delta u \, ds = \Gamma_b$$

and when $0 < |y| < \left|\frac{a^2}{b/2}\right|$ the strength of the image vortex located at $\frac{a^2}{b/2}$ is increased by π

$$\phi_u = -\phi_l = \frac{\Gamma_b}{2\pi}\left[\tan^{-1}\frac{\sqrt{a^2 - y^2}}{y - \frac{b}{2}} - \tan^{-1}\frac{\sqrt{a^2 - y^2}}{y + \frac{b}{2}} - \left(\pi + \tan^{-1}\frac{\sqrt{a^2 - y^2}}{y - \frac{a^2}{b/2}}\right) + \tan^{-1}\frac{\sqrt{a^2 - y^2}}{y + \frac{a^2}{b/2}}\right] = \frac{1}{\pi}\Gamma_b\left[\tan^{-1}\frac{2\frac{b}{2}\sqrt{a^2 - y^2}}{\left(\frac{b}{2}\right)^2 - a^2} - \frac{\pi}{2}\right]$$

and

$$\oint \Delta u \, ds = 0$$

Then, from equation (2), the lateral lift distribution of the induced lift can be written

$$\frac{dL_f}{dy} = \rho U_\infty \Gamma_b \left[1 - \frac{2}{\pi} \tan^{-1} \frac{2\frac{b}{2}\sqrt{a^2 - y^2}}{\left(\frac{b}{2}\right)^2 - a^2} \right] \qquad (-a < y < a) \qquad (3)$$

and after integration over y

$$L_f = 2\rho U_\infty \Gamma_b \left(a - \frac{a^2}{b/2} \right) \qquad (4)$$

which are the same as the expressions obtained by Lennertz for dL_f/dy and the total fuselage lift L_f. The components of L_f and dL_f/dy due to the additional potential must therefore be zero.

The longitudinal lift distribution on the cylinder calculated by Lennertz, which included the effect of the additional potential as well as the vortex potential, is slightly different from that which would be calculated due to the effect of the vortex potential alone. However, both distributions are symmetrical about the axis of the bound vortex. The longitudinal center of pressure of the lift due to the vortex potential must be at the bound-vortex axis because the longitudinal velocities induced on the surface of the cylinder by the bound vortex are the same in front and in back of the bound vortex as noted before. That the longitudinal center of pressure of the lift due to the vortex potential and the additional potential must be at the axis of the bound vortex as the Lennertz calculations show (although he does not say this explicitly) can be shown as follows:

Superposition of infinite vortices canceling the semi-infinite trailing vortices of figure 2(a) as shown in figure 2(b) will not change the longitudinal lift distribution on the cylinder since no longitudinal velocities are induced. It is apparent that the system is the same as before, with the direction of the trailing legs of the horseshoe vortices

reversed; therefore, the longitudinal distribution on the infinite cylinder must be symmetrical about the axis of the bound vortex, since, if it were not, the longitudinal lift distributions on the cylinders in figures 2(a) and 2(b) would be different.

From the analysis in this section of the wing and cylinder combination it can be seen that, for calculating the lift on the cylinder, its lateral distribution, and the longitudinal center of pressure, it is necessary to consider only the effect of the vortex potential. This lift due to the vortex potential will be referred to hereinafter as the "induced lift."

Simplified representation of the wing-fuselage combination.- In this paper, the wing-fuselage combination will be represented by a system of discrete horseshoe vortices and images, so that configurations with wings of arbitrary plan form may be treated. It is necessary to superimpose two pairs of horseshoe vortices of the type shown in figures 1 and 3 to obtain the vortex-image system of figure 4. The vortex-image system of figure 4 can be used to represent wings of arbitrary plan form in the manner shown in figure 5 by locating the bound vortices on the wing quarter-chord line or by distributing them over the wing surface in the same manner. Since the discrete horseshoe vortex becomes a doublet line as the length of the bound leg approaches zero, it is also possible to represent the wing by a continuous distribution of doublets.

Figure 3 shows the larger pair of vortices with span $2(y_n + s)$ and strength $+\Gamma$ near the smaller pair of span $2(y_n - s)$ and strength $-\Gamma$. When the bound legs of the smaller are moved to coincide with the bound legs of the larger, the net vortex strength along the section where they coincide is zero, and the remaining sections of the larger bound legs form the bound legs of the desired system (see fig. 4). From equations (3) and (4), the lateral distribution of the induced lift and the total induced lift for the vortex-image system shown in figure 4 are given by the following expressions:

$$\frac{\Delta\left(\frac{dL_f}{dy}\right)}{q\bar{c}} = \left(\frac{cc_l}{\bar{c}}\right)_n \frac{2}{\pi}\left[\tan^{-1}\frac{2(y_n - s)\sqrt{a^2 - y^2}}{(y_n - s)^2 - a^2} - \tan^{-1}\frac{2(y_n + s)\sqrt{a^2 - y^2}}{(y_n + s)^2 - a^2}\right] \quad (5)$$

$$\frac{\Delta L_f}{qS} = \left(\frac{cc_l}{\bar{c}}\right)_n \left[s^* \frac{2a^2}{y_n^2 - s^2} \right] \tag{6}$$

where $\left(\frac{cc_l}{\bar{c}}\right)_n$ is the loading coefficient on the wing at the station y_n.

Since it is known that the longitudinal center of pressure of the induced lift (and total lift) for each pair of horseshoe vortices and images is still located at the axis of the bound vortex, it is possible by superposition to calculate the pitching moment on the fuselage in the presence of a wing of arbitrary plan form if the lift distribution on the wing is known, although the complete longitudinal lift distribution cannot be calculated unless the component of loading due to the additional potential is calculated. The total induced lift and its lateral lift distribution can also be calculated by superposition. The method is discussed in one of the following sections, and an illustrative example is given in the appendix.

Effect of Finite Fuselage Length on the Induced Lift

To obtain an estimate of the error involved in the assumption of the foregoing analysis that the fuselage is infinitely long, an approximate calculation will be made of the effect of slenderness ratio on the induced lift of an ellipsoid of revolution combined with an infinite vortex. The limiting case of the spherical fuselage is treated first in the manner of Vandrey (ref. 4), and then the general case is treated.

Calculation of the lift on a sphere-vortex combination.- The potential of the sphere combined with an infinite vortex (fig. 6(a)) is written

$$\Phi = \frac{\Gamma_b}{2\pi} \tan^{-1} \frac{z}{x} + U_\infty x \left[1 + \frac{1}{2} \frac{a^3}{\left(\sqrt{x^2 + y^2 + z^2}\right)^3} \right] \tag{7}$$

where the potential for the sphere in the free stream is

$$\Phi_1 = U_\infty x \left[1 + \frac{1}{2} \frac{a^3}{\left(\sqrt{x^2 + y^2 + z^2} \right)^3} \right] \tag{8}$$

and the potential for the vortex is

$$\Phi_2 = \frac{\Gamma_b}{2\pi} \tan^{-1} \frac{z}{x} \tag{9}$$

The lift on a section of the sphere in the plane $y = \text{Constant}$ is

$$\frac{dL_f}{dy} = \int_{-\sqrt{a^2-y^2}}^{\sqrt{a^2-y^2}} \left(p_u - p_l \right) dx \tag{10}$$

where p_u and p_l are the pressures on the upper and lower surfaces, respectively. From Bernoulli's equation,

$$p = p_o + \frac{1}{2}\rho \left[(u + \Delta u)^2 + (v + \Delta v)^2 + (w + \Delta w)^2 \right] \tag{11}$$

and

$$p_u - p_l = 2\rho(u\,\Delta u + w\,\Delta w)$$

where Δu, Δv, and Δw are the velocities induced by the vortex on the upper half of the sphere and u, v, and w are the local velocities on the surface of the sphere. Thus

$$\left.\begin{aligned} \Delta u &= \frac{\Gamma_b}{2\pi} \frac{z}{a^2 - y^2} \qquad \Delta w = \frac{\Gamma_b}{2\pi} \frac{x}{a^2 - y^2} \\ u &= \frac{3}{2} U_\infty \frac{a^2 - x^2}{a^2} \qquad w = \frac{3}{2} U_\infty \frac{xz}{a^2} \end{aligned}\right\} \tag{12}$$

The lift on the section at y = Constant is

$$\frac{dL_f}{dy} = \frac{3}{2}\frac{\Gamma_b}{\pi}\frac{\rho U_\infty}{a^2 - y^2}\int_{-\sqrt{a^2-y^2}}^{\sqrt{a^2-y^2}} z\,dx \qquad (13)$$

which may be written in the form

$$\frac{dL_f}{dy} = \rho U_{max}\int_{-f(y)}^{f(y)} 2\,\Delta u\,dx \qquad (14)$$

since

$$\Delta u = \frac{\Gamma_b}{2\pi}\frac{z}{a^2 - y^2}$$

and since

$$u = U_{max}$$

when $x = 0$, so that

$$U_{max} = \frac{3}{2}U_\infty$$

For an infinite cylinder with an infinite vortex, equation (14) will also hold. In this case

$$U_{max} = U_\infty$$

$$\Delta u = \frac{\Gamma_b}{2\pi}\frac{\sqrt{a^2 - y^2}}{a^2 - y^2 + x^2}$$

and

$$f(y) = \infty$$

From equation (13) or (14) the lift obtained for the sphere is

$$\frac{dL_f}{dy} = \frac{3}{4}\rho U_\infty \Gamma_b$$

and for the cylinder

$$\frac{dL_f}{dy} = \rho U_\infty \Gamma_b$$

Equation (14) gives the exact result for the case of the sphere with an infinite vortex and the same result as the method of Lennertz for the case of an infinite cylinder with an infinite vortex. It is suggested, therefore, that equation (14) may be used to obtain a qualitative estimate for the intermediate case of an ellipsoid of revolution having a slenderness ratio between 1 and infinity. This assumption will be made in the following section and it will be shown that the value obtained for the induced lift by using equation (14) is very close to that obtained by the more accurate mathematical treatment of Vandrey (ref. 4) for the case of an ellipsoid having a slenderness ratio of 5.

Calculation of the lift on a combination of an ellipsoid with an infinite vortex.- From equation (14) the local lift on the ellipsoid is written

$$\frac{dL_f}{dy} = \rho U_{max} \int_{-f(y)}^{f(y)} 2\,\Delta u\,dx \tag{15}$$

From figure 6(b),

$$\left.\begin{aligned} f(y) &= d\sqrt{1 - \left(\frac{y}{a}\right)^2} \\ \Delta u &= \frac{\Gamma_b}{2\pi} \frac{a\sqrt{1 - \left(\frac{y}{a}\right)^2 - \left(\frac{x}{d}\right)^2}}{x^2 + a^2\left[1 - \left(\frac{y}{a}\right)^2 - \left(\frac{x}{d}\right)^2\right]} \end{aligned}\right\} \tag{16}$$

The integration indicated in equation (14) yields

$$\frac{1}{\rho U_\infty \Gamma_b}\frac{dL_f}{dy} = \frac{U_{max}/U_\infty}{1 + \frac{a}{d}} \tag{17}$$

The values of U_{max}/U_∞ given as a function of the slenderness ratio in reference 5 are shown in figure 7.

Figure 8 shows a plot of $\frac{1}{\rho U_\infty \Gamma_b}\frac{dL_f}{dy}$ against d/a. The result of a calculation by Vandrey for the case of an ellipsoid with $\frac{d}{a} = 5$ is shown to fall near the curve in figure 8. Since Vandrey's calculations appear to be accurate to 0.05, the agreement may be even better than is indicated in figure 8. Vandrey's results are obtained by difficult computations for each body separately, and his method does not yield a general expression similar to equation (17).

Figure 8 indicates that the induced lift on the ellipsoids having high slenderness ratios ($d/a > 5$) is about 90 percent of the induced lift on the infinite cylinder. Since the fuselage is similar effectively to a semi-infinite cylinder because of the wake which extends behind it, the loss in lift due to the finite fuselage length is about half of that indicated by the calculation for the ellipsoid of revolution. The value of induced lift obtained by assuming the fuselage to be an infinite cylinder may be multiplied by the factor $\frac{1}{2}\left(1 + \frac{U_{max}/U_\infty}{1 + \frac{a}{d}}\right)$ to correct for the finite fuselage length; however, this approximate correction can usually be neglected since it is nearly unity for most practical slenderness ratios. Since the correction is small, it is assumed that it may be applied directly for the finite-wing case without introducing significant error, so that the factor $\frac{1}{2}\left(1 + \frac{U_{max}/U_\infty}{1 + \frac{a}{d}}\right)$ is to be multiplied by equations (5) and (6) to correct for finite fuselage length.

APPLICATION OF SIMPLIFIED MATHEMATICAL MODEL TO CALCULATION OF THE AERODYNAMIC LOADING AND DOWNWASH

In the following sections, the method for calculating the induced lift will be described and discussed and methods for calculating the spanwise loading on the wing and the downwash will be outlined. The methods for calculating the downwash and spanwise lift distribution are not rigorous since the effect of the additional potential, which has not yet been calculated, must be approximated by a simple correction. Although the validity of the correction must depend on experimental verification, it is believed to be adequate, and the exact value of the additional potential may be incorporated into the method immediately when it is calculated.

Method for Calculating the Induced Lift on the Fuselage

If the lift distribution on the wing in the presence of the fuselage is known, say from reference 6 or the method outlined in the following section (see fig. 9), the induced lift may be calculated very simply. A sample numerical calculation is shown in the appendix. It is only necessary to substitute into equations (5) and (6) the value of loading coefficient, $\frac{cc_l}{\bar{c}}$, for each of the discrete horseshoe vortices. The values of the increments of the lateral lift distributions $\Delta \frac{dL_f}{dy}$ on the fuselage due to all of the horseshoe vortices and their images obtained from equation (5) are superimposed to get the complete lateral lift distribution dL_f/dy. The increment of total lift for each pair of horseshoe vortices and images ΔL_f acts at the bound-vortex axis, and the longitudinal center of pressure of the total lift L_f is obtained simply by dividing the sum of the moments of the incremental total lifts ΔL_f by the total lift L_f (the sum of the increments ΔL_f).

The results of the calculation for the lateral distribution and longitudinal center of pressure carried out in the appendix are presented in figures 10 and 11, respectively. Figure 11 shows the increment of total lift ΔL_f contributed by each pair of vortices and images and it can be seen that the contribution to the total lift L_f due to the outboard part of the wing (the contributions farthest aft in the side view) are small compared to the contribution of the inboard part of the wing. The induced lift on the fuselage has also been calculated by using the wing-alone spanwise lift distribution shown in figure 9;

that is, the effect of the fuselage on the wing is neglected. It can be seen in figures 10 and 11 that, although there is about a 10-percent increase in the magnitude of dL_f/dy and L_f due to the effect of the fuselage on the wing, the lateral and longitudinal load distribution on the fuselage is practically unaffected. The correction for finite length has not been included in the calculations. Its only effect would have been to decrease the magnitude of the lift, but it would not alter the lateral or longitudinal distribution.

The total lift and moment on the fuselage can be obtained by adding the components of lift and moment due to the induced lift to the components of lift and moment due to the local angle of attack of the fuselage (which can be calculated as shown in ref. 2). The lift and moment on the part of the wing outboard of the fuselage wall calculated by the method of reference 6 or the method of this paper (described in a later section) may then be added to the lift and moment on the fuselage to get the total lift and moment on the combination.

Outline of Method for Calculating the Lift on the Wing in the Presence of the Fuselage

The lift distribution on the wing will be calculated by equating the downwash angle induced at the three-quarter-chord line by the horseshoe vortices centered on the quarter-chord line (see fig. 5) to the local angle of attack on the three-quarter-chord line at several points along the span. Since the boundary conditions on the fuselage are not completely satisfied by the vortex-image system of figure 5 in the region near the bound vortex, it is necessary to resort to certain approximations in calculating the downwash. Calculation of the exact values of these downwash functions would require the calculation of the additional potential which involves a great deal of time and effort, but if such calculations were made, the values could be used directly in the present method and the restrictions suggested below would be eliminated.

The approximations described in the following sections improve as the longitudinal distance from the downwash points to the bound vortex increases so that this method is considered to be best-suited for configurations having fairly small ratios of diameter to root chord, say for straight wings with $\frac{\text{Diameter}}{\text{Root chord}} \leq \frac{1}{2}$ and for swept wings with $\frac{\text{Diameter}}{\text{Root chord}} \leq \frac{1}{3}$. Calculations of the aerodynamic loading on a wing and tip-tank combination, using a method corresponding to the one described herein with the downwash points located about 1 tip-tank diameter behind

the bound vortex $\left(\frac{\text{Diameter}}{\text{Tip chord}} \approx \frac{1}{2}\right)$, have been found to yield results in good general agreement with experimental results.

Downwash in region near the wing bound vortex.- Although the boundary conditions are satisfied completely only at infinity, the trailing legs of a single pair of horseshoe vortices and images also satisfy the boundary conditions on the cylinder in the plane perpendicular to the cylinder axis which passes through the bound legs of the horseshoe vortices. In addition, the boundary conditions on the cylinder are satisfied completely by the semi-infinite vortex-image system everywhere in the plane of the horseshoe vortex. Since the boundary conditions on the cylinder are satisfied exactly at the points noted, and are partly satisfied everywhere else, it will be assumed that the downwash due to the trailing vortices may be calculated approximately, at least in the plane of the horseshoe vortex, without introducing any correction factor.

It will be necessary, however, to use a correction factor in calculating the downwash due to the real and image bound vortices which have the greatest tendency to violate the boundary condition of zero velocity normal to the surface of the cylinder. It will be assumed that, along a line parallel to the bound vortex, the effect of the cylinder on the vertical flow induced by the bound vortex will be the same as its effect on a two-dimensional uniform rectilinear flow, so that the downwash induced by the bound vortices on that line is increased by the factor $1 + \frac{a^2}{y_a^2}$.

The downwash angle at a point at $y = y_a$ and $x = x_a$ (shown in fig. 4) is then written

$$\alpha_a = \frac{1}{4\pi A} \frac{b}{2s} \sum_n \gamma_n \left[F_n(x,y,0) + G_n(x,y,0) \left(1 + \frac{a^2}{y_a^2} \right) \right] \tag{18}$$

where the downwash factor due to the trailing vortices F_n and the downwash factor due to the bound vortices G_n may be calculated by the Biot-Savart law.

The function F_n is the sum of four terms, each having the form

$$\frac{1}{\bar{y}_n - \bar{y}_a + 1}\left[\frac{\bar{x}_a - \bar{x}_n}{\sqrt{\left(\bar{y}_n - \bar{y}_a + 1\right)^2 + \left(\bar{x}_a - \bar{x}_n\right)^2}} + 1\right] -$$

$$\frac{1}{\bar{y}_n - \bar{y}_a - 1}\left[\frac{\bar{x}_a - \bar{x}_n}{\sqrt{\left(\bar{y}_n - \bar{y}_a - 1\right)^2 + \left(\bar{x}_a - \bar{x}_n\right)^2}} + 1\right]$$

(the term corresponding to the trailing legs of the horseshoe vortex centered at $y = y_n$) and the function G_n is the sum of four terms, each having the form

$$\frac{1}{\bar{x}_a - \bar{x}_n}\left[\frac{\bar{y}_n - \bar{y}_a + 1}{\sqrt{\left(\bar{y}_n - \bar{y}_a + 1\right)^2 + \left(\bar{x}_a - \bar{x}_n\right)^2}} - \frac{\bar{y}_n - \bar{y}_a - 1}{\sqrt{\left(\bar{y}_n - \bar{y}_a - 1\right)^2 + \left(\bar{x}_a - \bar{x}_n\right)^2}}\right]$$

(the term corresponding to the bound leg of the horseshoe vortex centered at $y = y_n$).

Scheme for calculating spanwise lift distribution on the wing.- The lift distribution on the wing is calculated by equating the downwash angle on the wing induced by the vortex-image system to the local angle of attack on the three-quarter-chord line of the wing at n points as in reference 6. Thus equation (18) is written for each of the n stations, and the simultaneous equations can then be solved for γ_n at n points on the span. The + marks in figure 5 indicate the points where the downwash is equated to the local angle of attack.

The effective angle of attack α_a is equal to the geometric angle of attack on the wing α_g plus the angle of attack induced by the fuselage

$$\alpha_a = \alpha_g + \alpha_f' \qquad (19)$$

and

$$\alpha_f' = \alpha_f\left(1 + \frac{a^2}{y_a^2}\right) - \alpha_f$$

$$= \alpha_f \frac{a^2}{y^2} \tag{20}$$

where α_f is the geometric angle of attack of the fuselage and the factor $1 + \frac{a^2}{y^2}$ takes into account the increase in the vertical velocity of the free stream in the neighborhood of the fuselage as calculated by assuming the fuselage to be an infinite cylinder in a two-dimensional uniform rectilinear flow of magnitude $V\alpha_f$.

The effect of finite fuselage length (referred to in ref. 6 as the "inflow effect") must be included separately by multiplying γ at each spanwise station by the factor $1 + 2\delta$ where δ is the ratio of the local increment of longitudinal velocity due to the fuselage to the free-stream velocity. As shown in reference 6, the factor $1 + 2\delta$ is used to account approximately for the small increase in dynamic pressure in the flow over the wing due to the increase in the local longitudinal velocity near the surface of a fuselage of finite length.

Outline of Method for Calculating the Downwash

The downwash calculations made in this section are for the case when the wing is at an angle of incidence with the fuselage at zero geometric angle of attack. The accuracy of the calculated results must be verified by experimental results; however, by comparison with results of downwash calculations for the wing alone, the results of the calculations for the downwash in back of the wing-fuselage combination may serve to give useful information regarding the effect of the wing-fuselage interference.

As was noted previously, the boundary conditions on the wing-fuselage combination are completely satisfied by the vortex-image system infinitely far behind the wing. At a great distance behind the wing, therefore, the theoretical value of the downwash can be calculated accurately for a given spanwise lift distribution. This calculation is simple, and the results may be useful for certain applications. However, the approximations made in the preceding section for calculating the downwash at the wing three-quarter-chord line may give more accurate results for the downwash calculated in the plane of the wing in the region nearer the bound vortex.

If the lift distribution on the wing is known, say from the method of reference 6, or the method outlined in this paper, the downwash angle in the plane $x = \infty$ may be calculated by adding the downwash due to each pair of trailing vortices and their images. Thus, from the Biot-Savart Law and figure 4, the downwash angle α_a at the point $y = y_a$, $z = z_a$, and $x = \infty$ is given as

$$\alpha_a = \frac{1}{2\pi As^*} \sum_n \gamma_n F_n \tag{21}$$

where

$$F_n = \frac{\bar{y}_n - \bar{y}_a + 1}{\left(\bar{y}_n - \bar{y}_a + 1\right)^2 + \bar{z}_a^2} - \frac{\bar{y}_n - \bar{y}_a - 1}{\left(\bar{y}_n - \bar{y}_a - 1\right)^2 + \bar{z}_a^2} +$$

$$\frac{\bar{y}_n + \bar{y}_a + 1}{\left(\bar{y}_n + \bar{y}_a + 1\right)^2 + \bar{z}_a^2} - \frac{\bar{y}_n + \bar{y}_a - 1}{\left(\bar{y}_n + \bar{y}_a - 1\right)^2 + \bar{z}_a^2} +$$

$$\frac{\bar{y}_a - \frac{\bar{a}^2}{\bar{y}_n} + 1}{\left(\bar{y}_a - \frac{\bar{a}^2}{\bar{y}_n} + 1\right)^2 + \bar{z}_a^2} - \frac{\bar{y}_a - \frac{\bar{a}^2}{\bar{y}_n} - 1}{\left(\bar{y}_a - \frac{\bar{a}^2}{\bar{y}_n} - 1\right)^2 + \bar{z}_a^2} +$$

$$\frac{\bar{y}_a + \frac{\bar{a}^2}{\bar{y}_n} + 1}{\left(\bar{y}_a + \frac{\bar{a}^2}{\bar{y}_n} + 1\right)^2 + \bar{z}_a^2} - \frac{\bar{y}_a + \frac{\bar{a}^2}{\bar{y}_n} - 1}{\left(\bar{y}_a + \frac{\bar{a}^2}{\bar{y}_n} - 1\right)^2 + \bar{z}_a^2} \tag{22}$$

and $\gamma_n = \left(cc_l/\bar{c}\right)_n$ is the local lift at station $\pm y_n$.

The representation of the wake by discrete vortices is satisfactory if the downwash is calculated at points halfway between the trailing legs $(y_a = y_n)$. The values calculated at these points may be faired to obtain a continuous spanwise distribution of downwash angle.

CONCLUDING REMARKS

For the purpose of calculating the longitudinal loading on the fuselage in subsonic flow, a midwing wing-fuselage combination has been represented by a system of discrete horseshoe vortices and images. Using this simplified mathematical model, a method for calculating the lift on the fuselage induced by the wing is presented and illustrated by a numerical example. This "induced lift" can be added to the lift on the part of the wing outboard of the fuselage and the lift on the fuselage due to the upwash induced by the wing to get the total loading on the wing-fuselage combination with an axisymmetrical fuselage and a wing of arbitrary plan form.

In addition to the method for calculating the induced lift, which is theoretically rigorous, methods for calculating the downwash far behind the wing and for calculating the spanwise lift distribution on the wing in the presence of the fuselage are outlined. In calculating the spanwise lift distribution on the wing, approximations are made to account for the effect of the "additional potential" so that the method is not rigorous. However, the effect of the additional potential may easily be incorporated into the method when it is calculated.

Langley Aeronautical Laboratory,
National Advisory Committee for Aeronautics,
Langley Field, Va.

APPENDIX

ILLUSTRATIVE EXAMPLE

A numerical example is given to illustrate the method presented in the body of the paper for calculating the induced lift on the fuselage.

Geometric characteristics of the midwing configuration used in the illustrative example.- The plan view of the wing-fuselage combination is essentially the same as shown in figure 5. The geometric data are

Aspect ratio	8
Taper ratio	0.45
Sweepback, deg	45
a^*	0.10
s^*	0.05

Spanwise loading on the wing in the presence of the fuselage.- The spanwise lift distribution on the wing in the presence of the fuselage tabulated below and shown in figure 9 is the same as the one obtained in reference 6 for a high midwing configuration. It is, however, qualitatively correct for the pure midwing case and is used to illustrate the procedure for obtaining the induced lift on the fuselage. The lift distribution on the wing in the presence of the fuselage plotted in figure 9 is tabulated as follows:

n	y_n^*	x_n^*	$\left(\frac{cc_l}{\bar{c}}\right)_n$
1	0.15	0.15	0.369
2	.25	.25	.366
3	.35	.35	.356
4	.45	.45	.338
5	.55	.55	.319
6	.65	.65	.300
7	.75	.75	.266
8	.85	.85	.241
9	.95	.95	.200

Longitudinal distribution of the induced lift.- Equation (6) which gives the lift on the fuselage due to a single pair of horseshoe vortices at $(x_n', \pm y_n')$ and their images can be written

$$\frac{\Delta L_f}{qS} = \left(\frac{cc_l}{\bar{c}}\right)_n s^* \frac{2}{y_n'^2 - s'^2} \tag{A1}$$

The total lift L_f/qS is then

$$\frac{L_f}{qS} = s^* \sum_n \left(\frac{cc_l}{\bar{c}}\right)_n \frac{2}{y_n'^2 - s'^2} \tag{A2}$$

The longitudinal center of pressure referred to the intersection of the quarter-chord line and the fuselage axis of symmetry (see fig. 5) is

$$x_{cp}' = \frac{\sum_n \left(\frac{cc_l}{\bar{c}}\right)_n \frac{2}{y_n'^2 - s'^2} x_n'}{\sum_n \left(\frac{cc_l}{\bar{c}}\right)_n \frac{2}{y_n'^2 - s'^2}} \tag{A3}$$

The computed values of L_f/qS and x_{cp}' are obtained from the values presented in the following table:

n	$\frac{2}{y_n'^2 - s'^2}$	$\left(\frac{cc_l}{\bar{c}}\right)_n \frac{2}{y_n'^2 - s'^2}$	$\left(\frac{cc_l}{\bar{c}}\right)_n \frac{2}{y_n'^2 - s'^2} x_n'$
1	1.000	0.369	0.554
2	.333	.122	.305
3	.168	.060	.210
4	.100	.034	.153
5	.066	.021	.116
6	.048	.014	.091
7	.036	.010	.075
8	.028	.007	.060
9	.022	.005	.048
		$\sum$ = 0.642	$\sum$ = 1.612

$$\frac{L_f}{qS} = 0.05 \sum_{1}^{9} \left(\frac{cc_l}{\bar{c}}\right)_n \frac{2}{y_n'^2 - s'^2}$$

$$= 0.032$$

$$x_{cp}' = \frac{\sum_{1}^{9} \left(\frac{cc_l}{\bar{c}}\right)_n \frac{2}{y_n'^2 - s'^2} x_n'}{\sum_{1}^{9} \left(\frac{cc_l}{\bar{c}}\right)_n \frac{2}{y_n'^2 - s'^2}}$$

$$= 2.51$$

The values of $s^*\left(\frac{cc_l}{\bar{c}}\right)_n \frac{2}{y_n'^2 - s'^2}$ are plotted as vectors in figure 11. The location of x_{cp}' is also shown.

Lateral distribution of the induced lift.- Equation (5) which gives the lateral distribution of the induced lift on the fuselage due to a single pair of horseshoe vortices at $(x_n', \pm y_n')$ and their images can be written

$$\frac{\Delta\left(\frac{dL_f}{dy}\right)}{q\bar{c}} = \frac{2}{\pi}\left(\frac{cc_l}{\bar{c}}\right)_n \left[\tan^{-1}\frac{2(y_n' - s')\sqrt{1 - y'^2}}{(y_n' - s')^2 - 1} - \tan^{-1}\frac{2(y_n' + s')\sqrt{1 - y'^2}}{(y_n' + s')^2 - 1}\right] \tag{A4}$$

The total lift at a station $\pm y'$ on the fuselage is then

$$\frac{\frac{dL_f}{dy}}{q\bar{c}} = \frac{2}{\pi}\sum_{n}\left(\frac{cc_l}{\bar{c}}\right)_n \left[\tan^{-1}\frac{2(y_n' - s')\sqrt{1 - y'^2}}{(y_n' - s')^2 - 1} - \tan^{-1}\frac{2(y_n' + s')\sqrt{1 - y'^2}}{(y_n' + s')^2 - 1}\right] \tag{A5}$$

The value of $\frac{\frac{dL_f}{dy}}{q\bar{c}}$ at $\pm y' = 0.25$ is calculated from the values in the following table (the lateral lift at any station $\pm y'$ can be calculated in a similar manner):

	(I)	(II)	
n	$\tan^{-1}\frac{2(y_n' - s')\sqrt{1 - y'^2}}{(y_n' - s')^2 - 1}$	$\tan^{-1}\frac{2(y_n' + s')\sqrt{1 - y'^2}}{(y_n' + s')^2 - 1}$	$\left(\frac{cc_l}{\bar{c}}\right)_n\left(\text{(I)} - \text{(II)}\right)_n$
1	1.571	0.918	0.241
2	.918	.633	.104
3	.633	.481	.054
4	.481	.387	.032
5	.387	.324	.020
6	.324	.279	.014
7	.279	.244	.010
8	.244	.217	.007
9	.217	.195	.005
			$\sum$ = 0.487

$$\frac{\frac{dL_f}{dy}}{q\bar{c}} = 0.637 \sum_{1}^{9} \left(\frac{cc_l}{\bar{c}}\right)_n \left(\text{(I)} - \text{(II)}\right)_n = 0.310$$

at $y' = 0.25$. The complete lateral lift distribution is shown in figure 10.

REFERENCES

1. Multhopp, H.: Aerodynamics of the Fuselage. NACA TM 1036, 1942.

2. Schlichting, H.: Calculation of the Influence of a Body on the Position of the Aerodynamic Centre of Aircraft With Sweptback Wings. TN No. Aero 1879, British R.A.E., Mar. 1947.

3. Lennertz, J.: Beitrag zur theoretischen Behandlung des gegenseitigen Einflusses von Tragfläche und Rumpf. Z.f.a.M.M., Bd. 7, Aug. 1927, pp. 249-276.

4. Vandrey, F.: Zur theoretischen Behandlung des gegenseitigen Einflusses von Tragflügel und Rumpf. Luftfahrtforschung, Bd. 14, Lfg. 7, Sept. 7, 1937, pp. 347-355.

5. Young, A. D., and Owen, P. R.: A Simplified Theory for Streamline Bodies of Revolution, and Its Application to the Development of High-Speed Low-Drag Shapes. R. & M. No. 2071, British A.R.C., 1943.

6. Zlotnick, Martin, and Diederich, Franklin W.: Theoretical Calculation of the Effect of the Fuselage on the Spanwise Lift Distribution on a Wing. NACA RM L51J19, 1952.

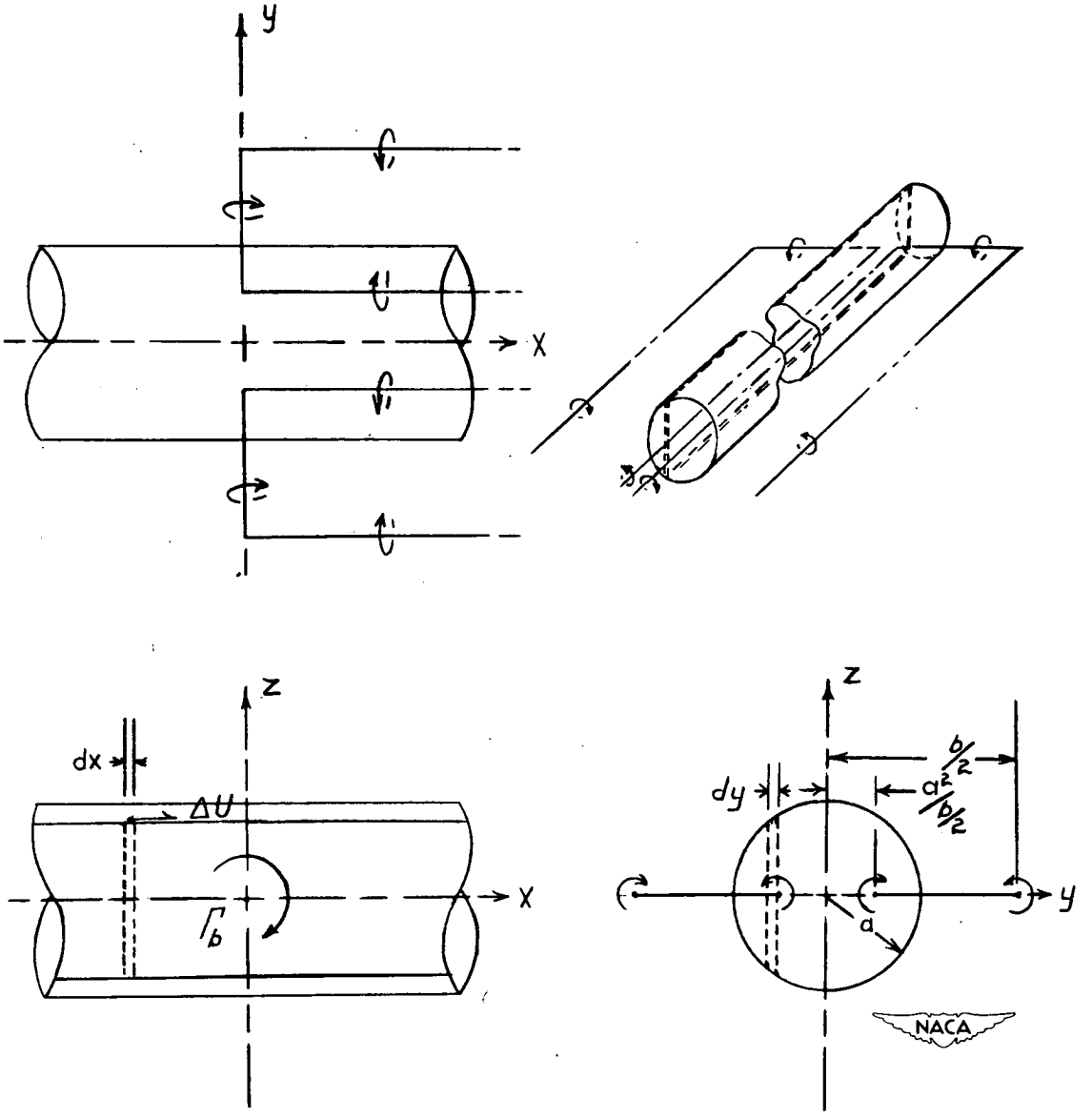

Figure 1.- Combination of horseshoe vortex and infinite cylinder.

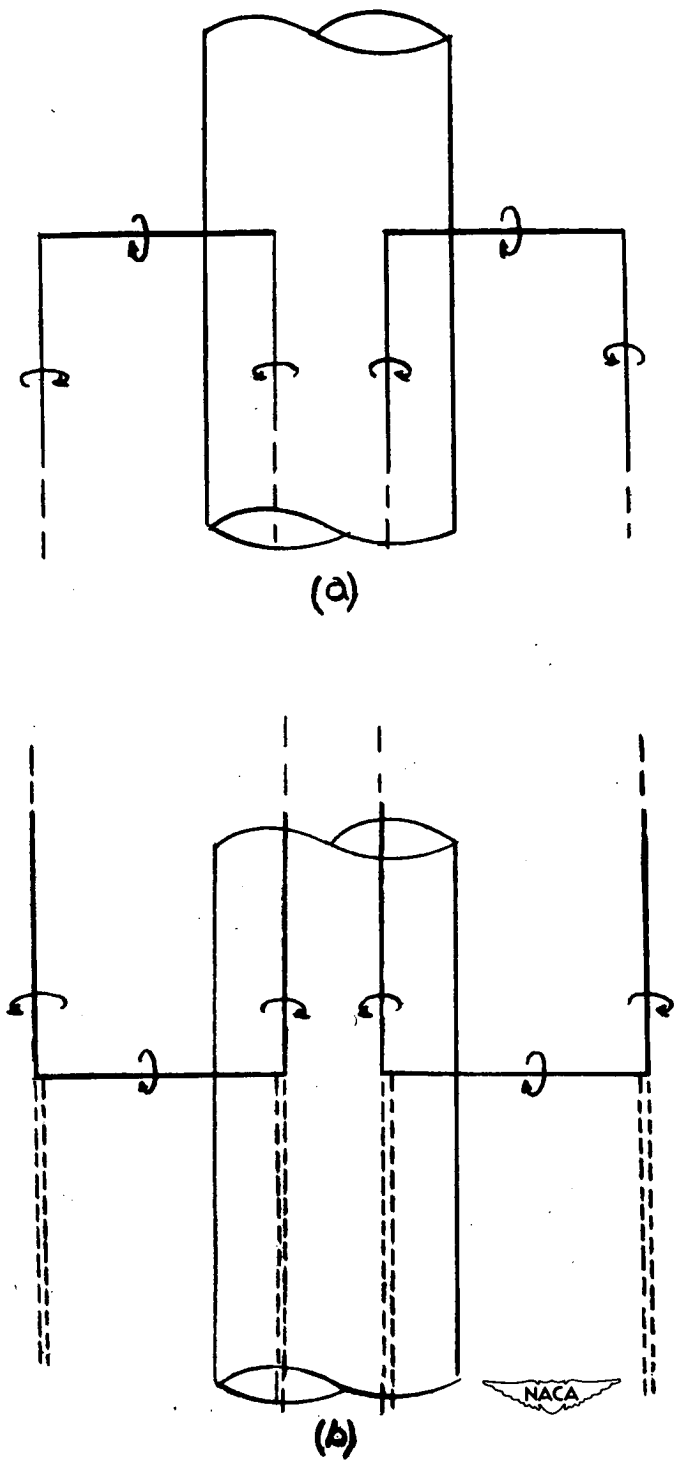

Figure 2.- Illustration showing superposition of infinite trailing vortices on cylinder and horseshoe vortex system.

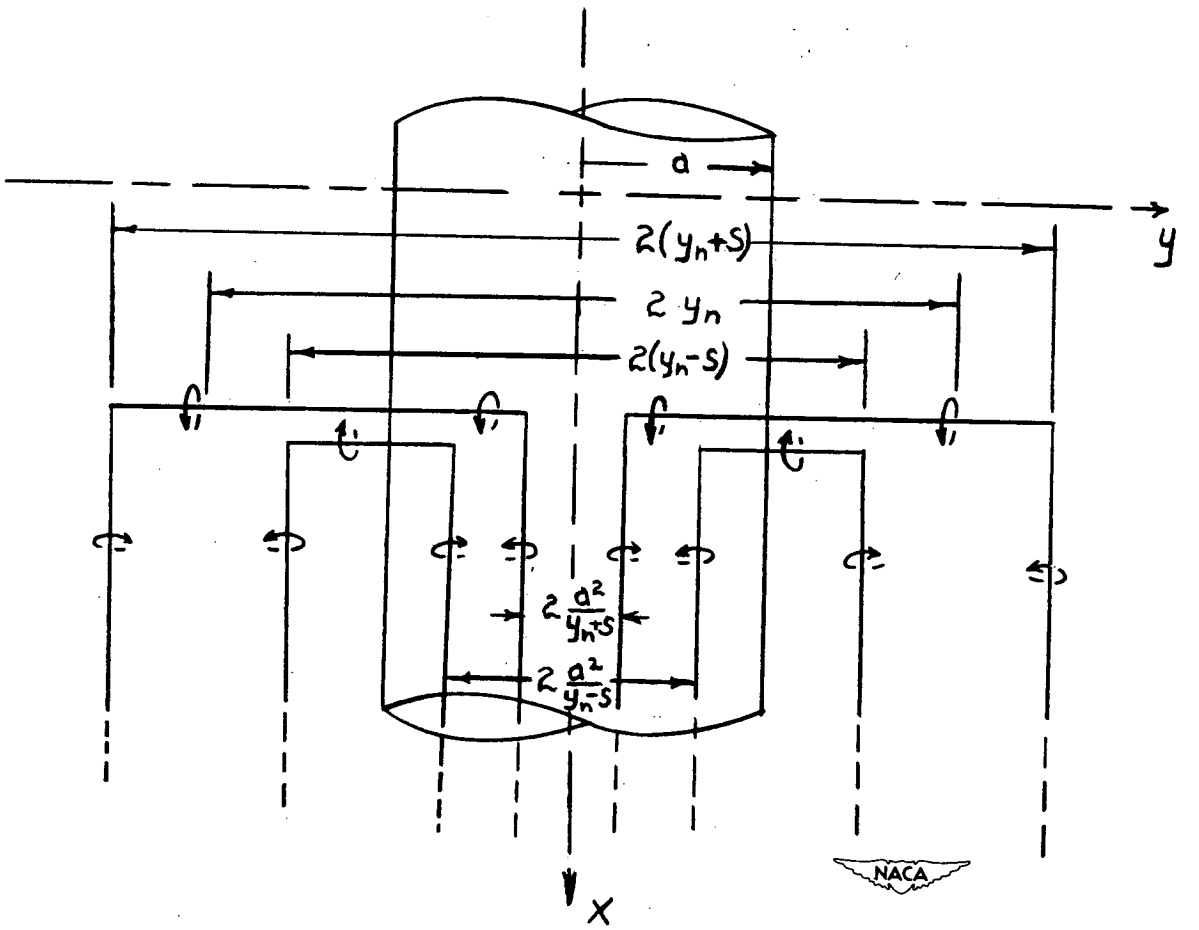

Figure 3.- Superposition of two unequal pairs of symmetrical horseshoe vortices to form a discrete horseshoe vortex-image system.

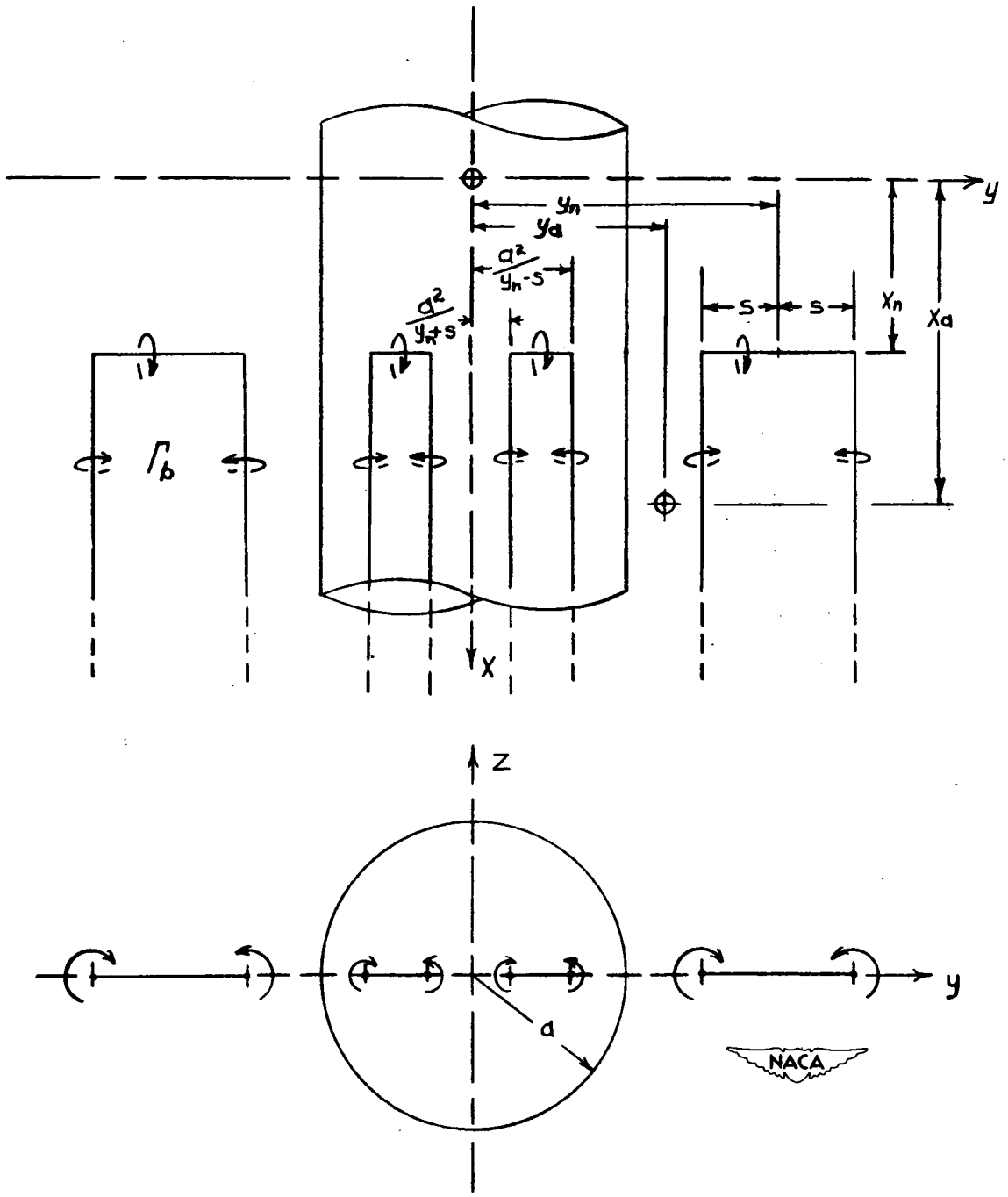

Figure 4.- Cylinder with a pair of symmetrically disposed horseshoe vortices and their images.

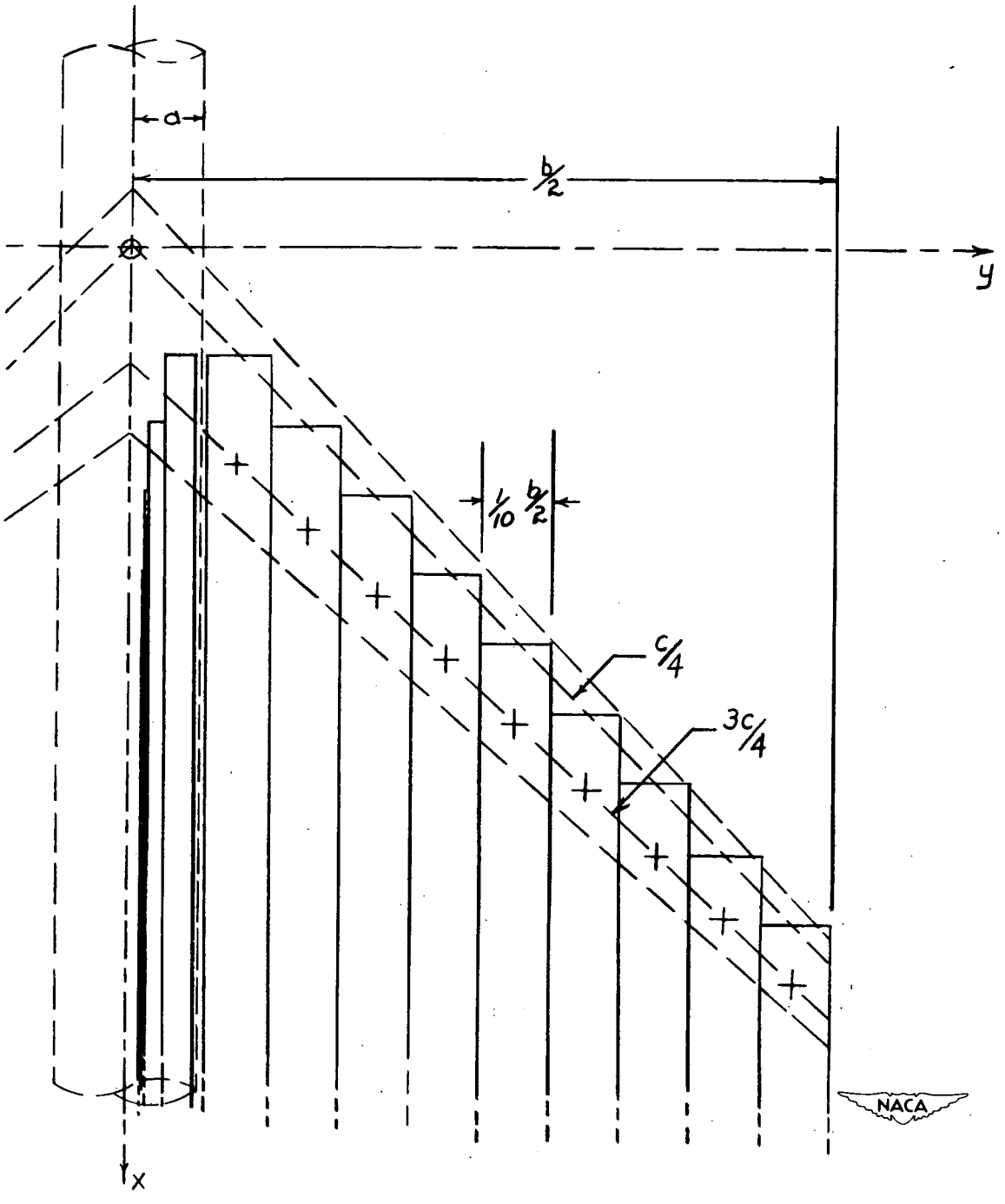

Figure 5.- Cylinder-wing combination. Sweepback angle, 45°; taper ratio, 0.45; A = 8; a* = 0.10.

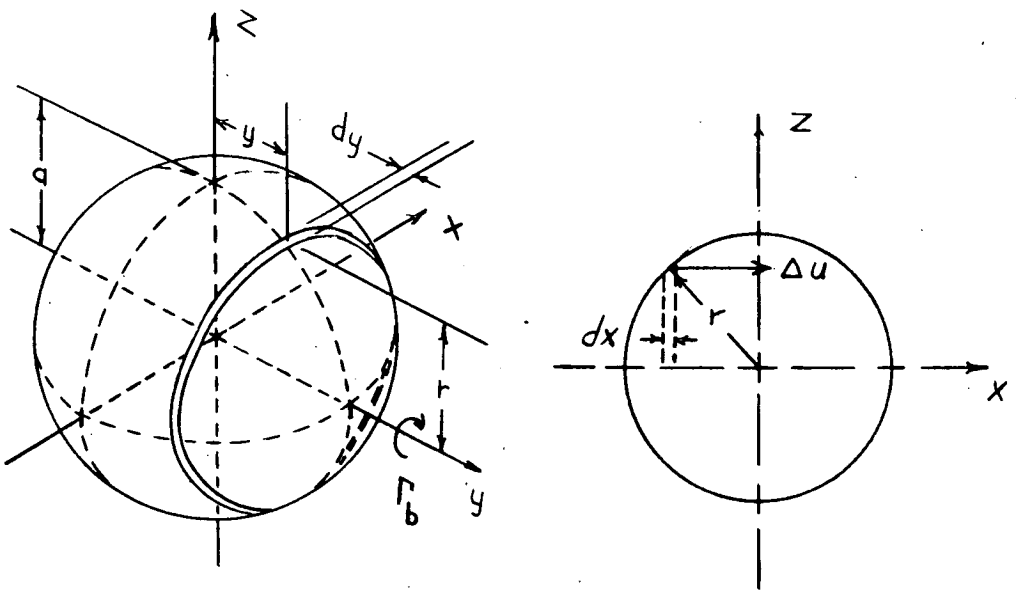

(a) Infinite-vortex—sphere configuration.

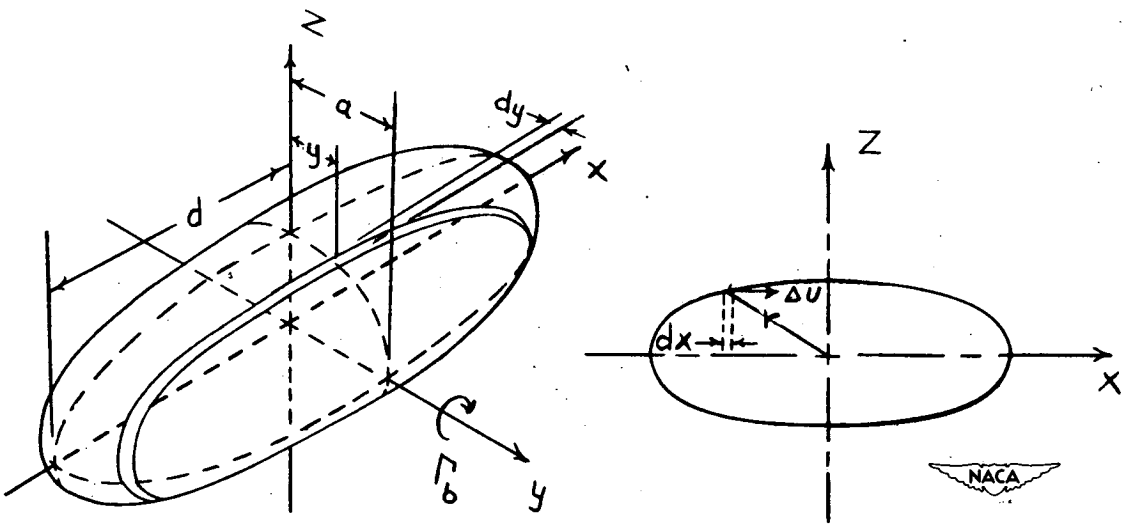

(b) Infinite-vortex—ellipsoid configuration.

Figure 6.- Illustrations of sphere with infinite vortex and ellipsoid with infinite vortex.

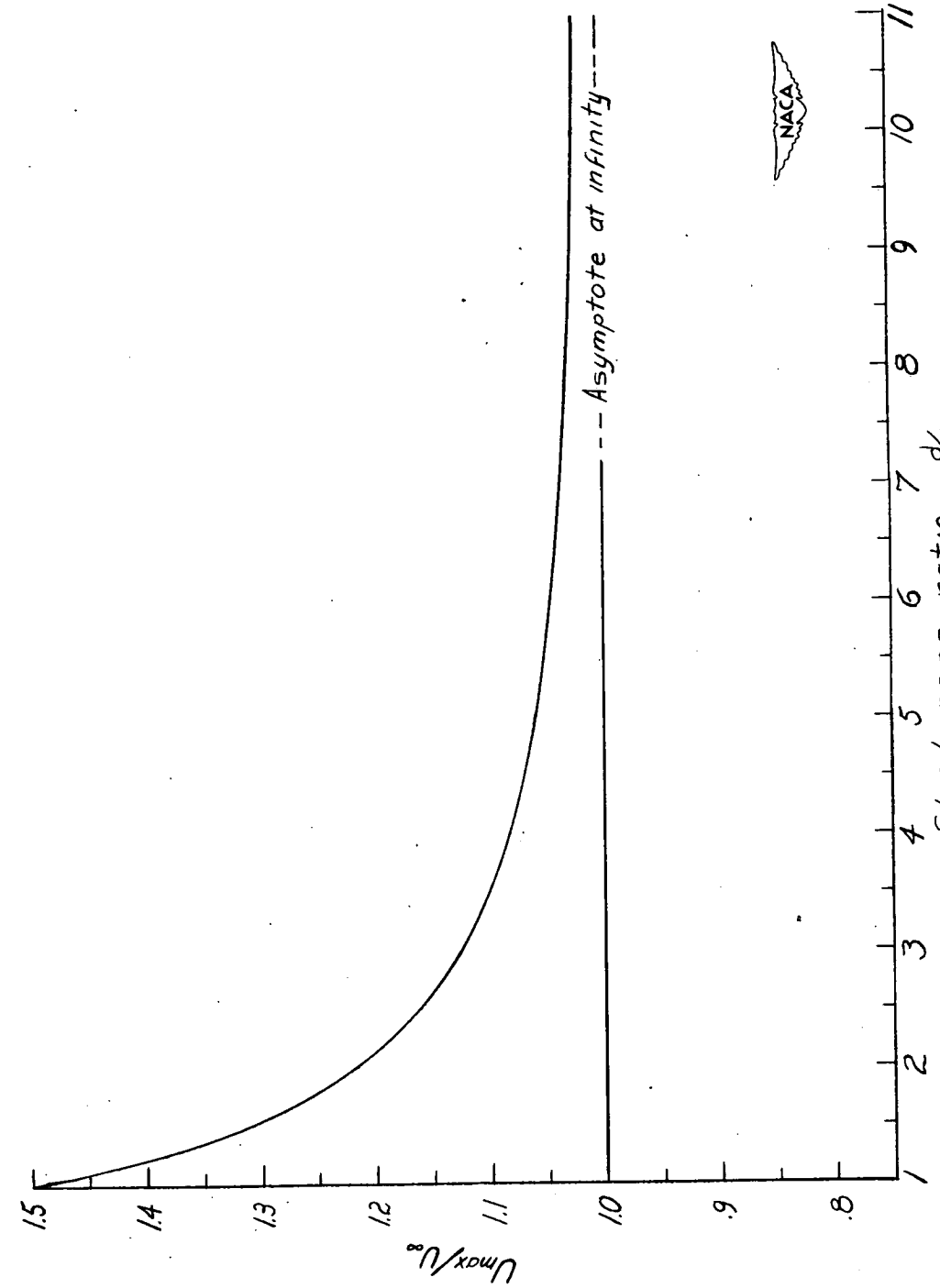

Figure 7.- Effect of slenderness ratio on the maximum velocity of flow past an ellipsoid of revolution.

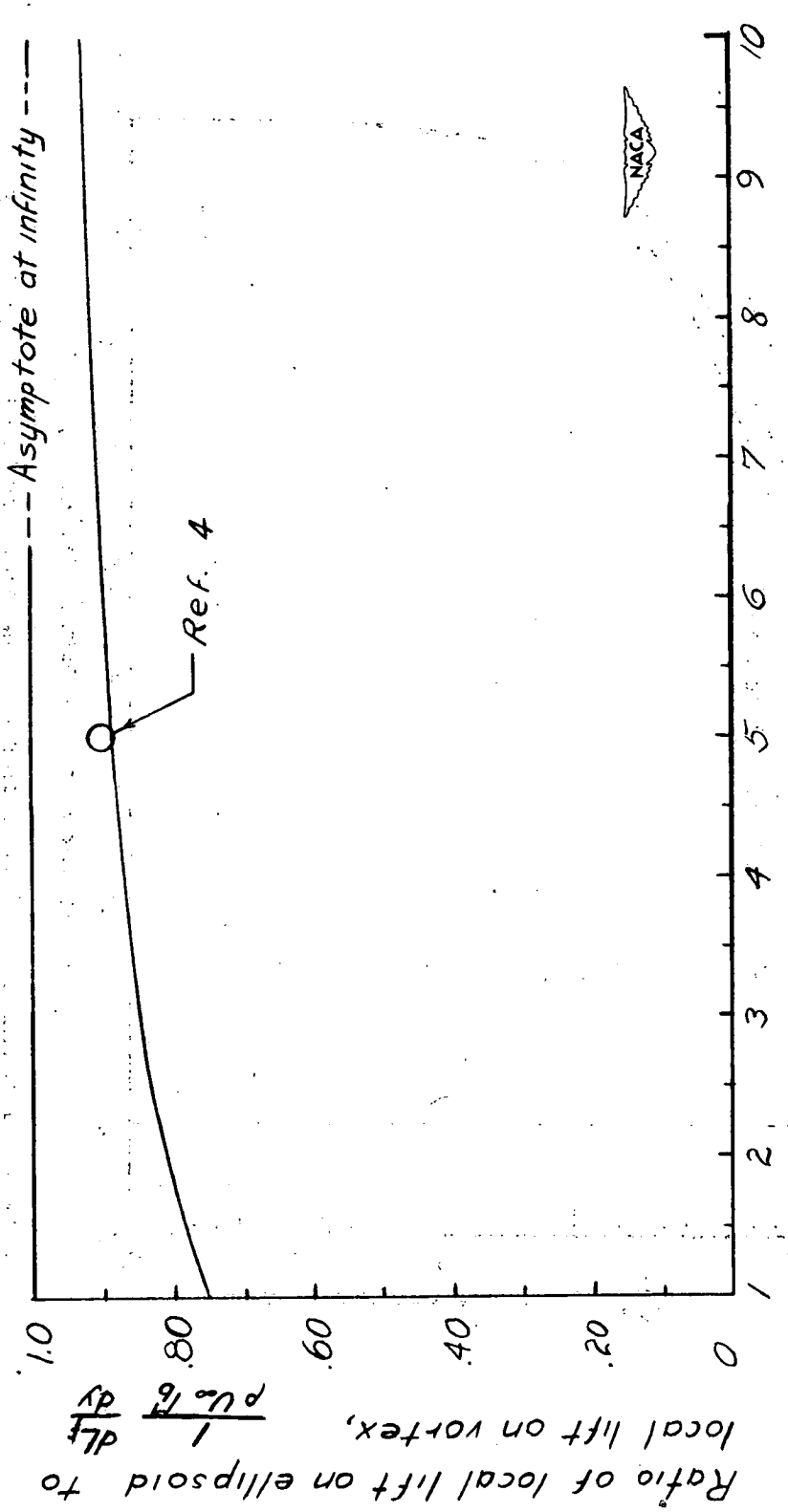

Figure 8.- Effect of slenderness ratio on the lift carried by an ellipsoid of revolution intersected by an infinite vortex having the strength Γ_b.

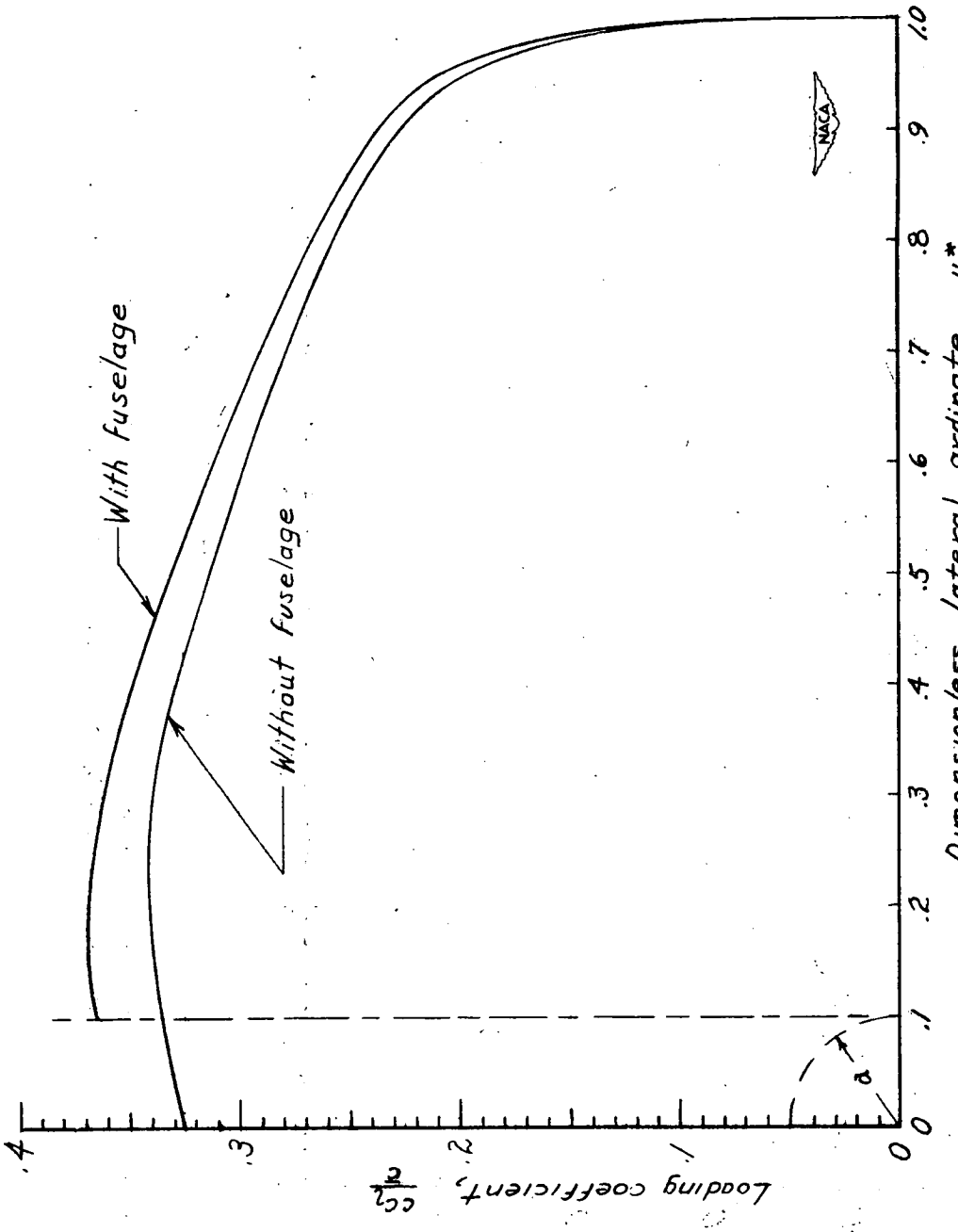

Figure 9.- Lateral lift distribution on wing alone and on a wing-fuselage combination. Sweepback angle, 45°; taper ratio, 0.45; A = 8; a* = 0.10.

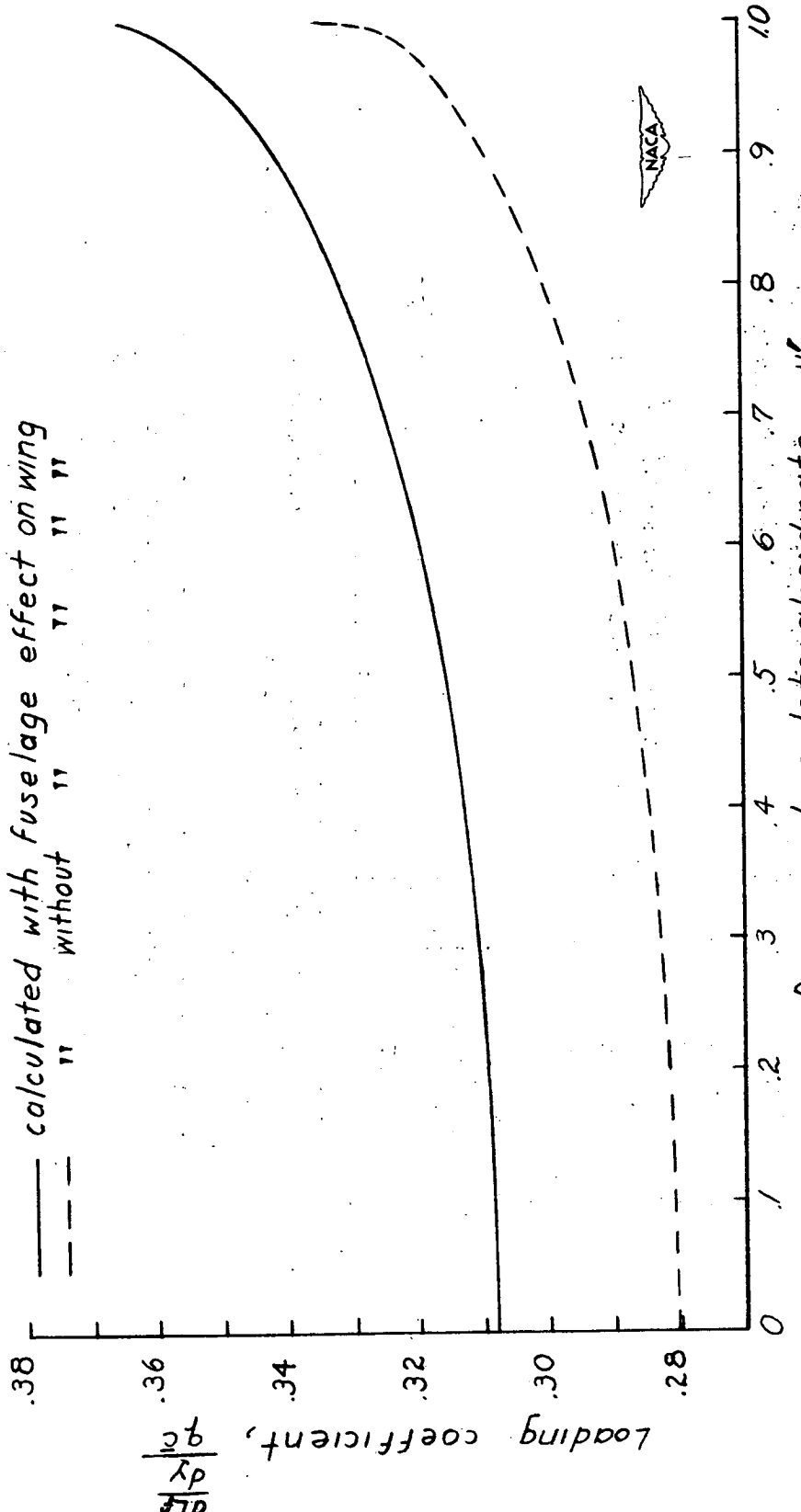

Figure 10.- Lateral distribution of induced lift on the fuselage in the presence of the wing. Sweepback angle, 45°; taper ratio, 0.45; A = 8; $a^* = 0.10$.

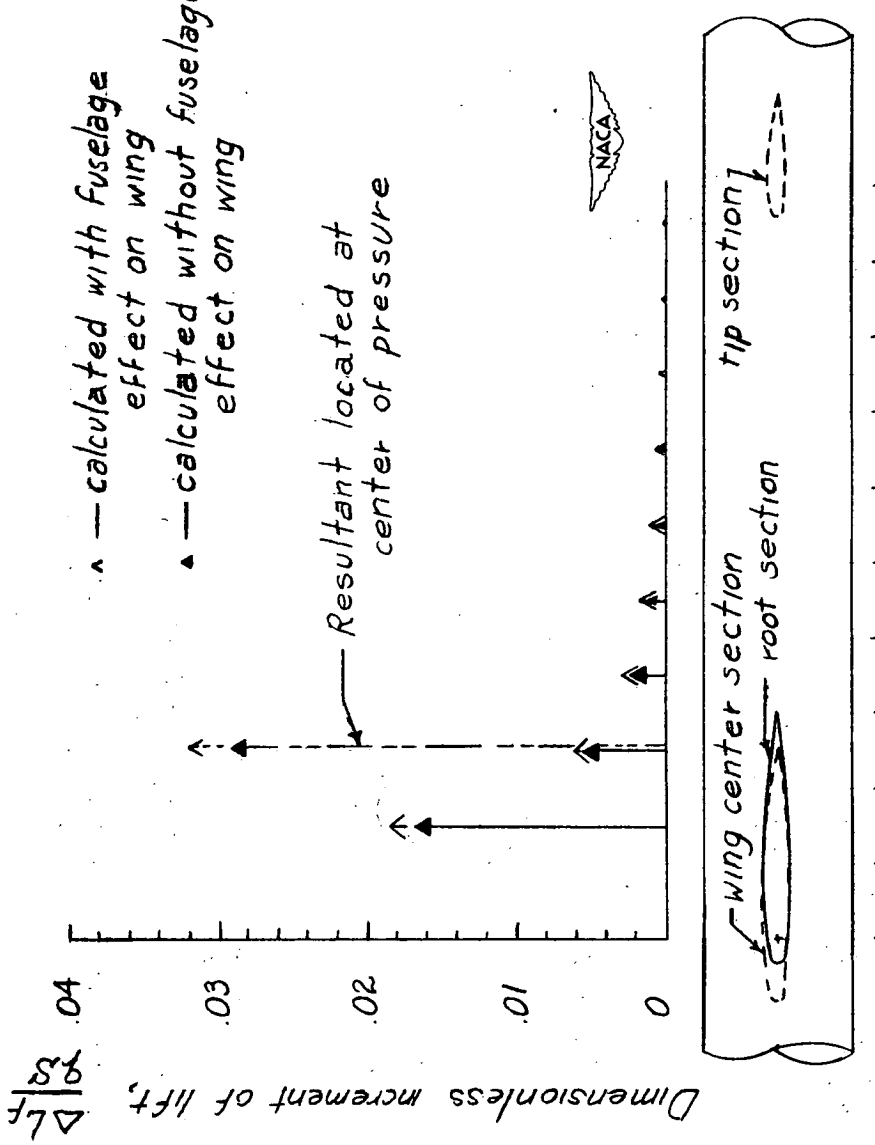

Figure 11.- Longitudinal distribution of induced lift on fuselage in the presence of the wing. Sweepback angle, 45°; taper ratio, 0.45; A = 8; $a^* = 0.10$.

NACA-Langley - 1-16-53 - 325